

Predissociation of the $4p\pi L^1\Pi$ Rydberg state of carbon monoxide

P. Cacciani^{a,*}, F. Brandi^b, J.P. Sprengers^b, A. Johansson^c, A. L'Huillier^c,
C.-G. Wahlström^c, W. Ubachs^b

^a Laboratoire PhLAM, CERLA FR 2416 CNRS, Université des Sciences et Technologies de Lille, 59655 Villeneuve d'Ascq, France

^b Department of Physics and Astronomy, Laser Centre, Vrije Universiteit, De Boelelaan 1081, 1081 HV Amsterdam, The Netherlands

^c Department of Physics, Lund Institute of Technology, P.O. Box 118, S-221 00 Lund, Sweden

Received 21 February 2002; in final form 22 May 2002

Abstract

Time-domain and frequency-domain spectroscopic experiments have been performed on the $(4p\pi)L^1\Pi$, $v=0$ Rydberg state in three isotopomers of carbon monoxide. Accurate values for the excited state lifetimes of the f-parity components have been determined: $\tau(^{12}\text{C}^{16}\text{O}) = 1.08 \pm 0.05$ ns, $\tau(^{13}\text{C}^{16}\text{O}) = 72 \pm 10$ ps and $\tau(^{13}\text{C}^{18}\text{O}) = 29 \pm 6$ ps. The spectral resolution in the frequency-domain experiment goes as far as the limit imposed by the natural lifetime; Q-branch lines, or f-parity components of the heavier isotopes, are resolved for the first time. Highly accurate transition frequencies are determined in a molecular beam experiment using comparison and interpolation with a saturated iodine reference standard. The results reveal a number of perturbations and predissociation mechanisms, displaying a high degree of complexity in the energetic region of the 4p Rydberg states of CO with strong isotopic effects. © 2002 Elsevier Science B.V. All rights reserved.

1. Introduction

The electronic structure and dynamics in the dissociation region of CO, i.e., at excitation energies of 10 eV and higher, is still associated with some unsolved problems [1]. The general finding that dissociation of carbon monoxide occurs via predissociation rather than via continuum absorption [2,3] has made the problem of the dissociation phenomenon in CO a very difficult one to

understand and quantify. Rydberg–valence interactions play an important role: the entire manifold of Rydberg states is known to interact with the repulsive part of a $D^1\Sigma^+$ potential, that supports some bound levels confined to large internuclear separation below the dissociation limit [4]. From an astrophysics perspective it is of importance to quantify the overall dissociation probability of CO and its isotopomers in the interstellar medium, where the molecules are subject to the stellar vacuum ultraviolet radiation field [5]. Hence the problem of dissociation of carbon monoxide has attracted the interest of several researchers in the past decade, who employed a wide variety of ex-

* Corresponding author. Fax: +33-32033-7020.

E-mail address: patrice.cacciani@univ-lille1.fr (P. Cacciani).

perimental techniques. In the initial models of interstellar photodissociation [3,5] isotopic fractionation was ascribed to radiation shielding effects in the interstellar medium. Recently some effects of rotational state dependent and isotope dependent predissociation rates have been observed in the laboratory [6–8], thus adding to the complexity.

In the present paper we focus on a single vibronic quantum state, the $4p\pi L^1\Pi$, $v = 0$ state. This state is exemplary for the problems encountered in explaining the dissociation dynamics: four different mechanisms of predissociation are required to explain the observed behavior. Experimentally, two advanced laser spectroscopic techniques are employed. The Amsterdam narrow-band extreme ultraviolet (XUV) laser facility is used to spectrally resolve the rotational structure of the dense Q-branch close to the natural linewidth. The Lund picosecond XUV-laser is used in a pump–probe scheme to determine the excited state lifetime in a time-delayed measurement. A major finding is the strong isotopic dependence of the lifetime of the $4p\pi L^1\Pi$, $v = 0$ Rydberg state: the $^{13}\text{C}^{16}\text{O}$ and $^{13}\text{C}^{18}\text{O}$ isotopomers are roughly an order of magnitude shorter lived than the main $^{12}\text{C}^{16}\text{O}$ isotopomer. Attempts were undertaken to also investigate the $4p\pi L^1\Pi$, $v = 1$ state. While the signals are too weak to record high resolution data some estimate of the lifetime can be inferred from direct time-domain measurements.

The present work builds upon a number of investigations on the $4p\pi L^1\Pi$, $v = 0$ state. The Amsterdam group used their coherent XUV source in various stages of sensitivity and resolution to study the $L^1\Pi$ of CO [9–11]. Eikema et al. [10] quantitatively investigated the isotope dependence as well as the rotational state dependence of the predissociation rate for the e-parity components, probed in P and R branches of the L–X(0,0) band. Subsequently Ubachs et al. [11] investigated the predissociation of the f-parity states with full resolution of the Q-branch lines. Similar as in a two-step laser excitation experiment by Drabbels et al. [12] the f-parity states were found to be predissociated, but at a rate much smaller than the e-parity states. In both [11] and in the study of Sekine et al. [13] using opto-galvanic spectroscopy, the Q(7) line was clearly missing; this phenomenon

is associated with enhanced predissociation of the $4p\pi L^1\Pi$, $v = 0$, $J = 7$, f-parity state. In the present study the Q(7) line is observed as a largely broadened feature and the perturbation around the $J = 7(f)$ level is analyzed in detail.

The group of Ebata have developed alternative laser-based methods, employing multi-step excitation, for an investigation of the Rydberg states of CO [14–16]. In recent publications they address the predissociation of the $4p\pi L^1\Pi$, $v = 0$ state from a different perspective. Using a pump–probe excitation scheme they were able to unravel the product channels in the dissociation processes, since a distinction can be made between the singlet channel leading to $\text{C}(^3\text{P}) + \text{O}(^3\text{P})$ and the triplet channel leading to $\text{C}(^1\text{D}) + \text{O}(^3\text{P})$. The dissociative decay of the f-parity levels in $4p\pi L^1\Pi$, $v = 0$ was ascribed to an interaction with the $2^1\Pi$ state, which was calculated by ab initio methods [17]. In addition, the observation of $\text{C}(^1\text{D})$ fragments for both parities suggests a possible interaction with triplet potentials $3^3\Pi$ and $2^3\Sigma^-$ as calculated by O’Neil and Schaefer [18].

Lifetimes of the $4p\pi L^1\Pi$, $v = 0$ state have been determined mainly from line broadening experiments [10–12,19]. While the resolution of these experiments was sufficient to quantify predissociation rates in the e-parity levels, the width of the f-parity levels was found to be close to the end of the dynamic range of the line broadening method, therewith increasing the uncertainty. In [11] a value of 1.0 ± 0.3 ns was obtained, while in [12] a value of 0.55 ns was reported. For this reason a direct time-domain measurement of the lifetime of $4p\pi L^1\Pi$, $v = 0$ was undertaken for several isotopomers, the results of which are presented here. The finding of much shorter lifetimes for the f-parity states of $^{13}\text{C}^{16}\text{O}$ and $^{13}\text{C}^{18}\text{O}$ led us also to reinvestigate the spectra of the L–X(0,0) bands of these isotopomers with the high resolution instrument.

2. Experimental methods

The measurements are performed with different XUV-laser sources at different sites. Direct time-domain determinations of excited state lifetimes

are performed with the picosecond XUV-laser source of the Lund Laser Centre. Its characteristics and the application in lifetime measurements of excited states of CO was reported before [6,8] and here only a few relevant parameters are given. XUV-pulses near 97 nm are produced via a non-linear wave mixing process involving the output of a distributed-feedback dye laser (DFDL) running at 775 nm, which is amplified in a titanium-sapphire bow-tie amplifier, and its second harmonic, effectively generating the 8th harmonic of the fundamental. The system has an estimated bandwidth of $\Delta\lambda_{\text{XUV}} \approx 0.01$ nm at the 8th harmonic. The pulse duration of the fundamental is found to be around 60 ps measured by a streak camera.

The XUV pulses are used in a pump-probe scheme, where the tunable XUV resonantly populates the $L^1\Pi$ state and the output of a frequency-doubled mode-locked Nd:YAG laser at 532 nm ionizes the CO molecules for signal recording. Variation of the time delay between XUV pulse and 532 nm pulses is set mechanically to yield temporal decay curves. The temporal resolution is limited by the convoluted duration of the two pulses, which is estimated at 160 ps. Details on the data collection procedures and the treatment of the data are described in [6].

The narrow-band tunable XUV-laser source of the Laser Centre Vrije Universiteit Amsterdam, and its application to spectral observations in CO, was also described before [7,8,11]. Nearly Fourier-transform limited nanosecond XUV pulses are produced by frequency-doubling and subsequent tripling of the output of a pulsed-dye-amplifier, which is seeded by a cw-ring dye laser at 581 nm. Absolute frequency calibration is performed by referencing to a recently established Doppler-free saturation I_2 -spectrum [20]. Relative frequency separations are derived from simultaneously recorded transmission fringes of a pressure and temperature stabilized etalon.

Signal is recorded from 1 XUV + 1 UV resonantly enhanced photoionization. The linewidth of the CO-resonances results from the combined effect of laser linewidth, natural lifetime broadening and residual Doppler broadening in the crossed beam configuration. Since the measurements are optimized to retain optimum signal for a study of

the weaker lines, the nozzle-skimmer distance in the molecular beam setup is reduced to only a few mm and the pressure conditions are chosen much higher than in previous study on the $4p\pi L^1\Pi$, $v = 0$ state [11]. Hence the effective width on the CO-resonances is larger than previously obtained; moreover a Doppler-broadened pedestal contributes to the spectral lines as a result of increased pressure in the interaction region.

3. Results and interpretation

3.1. Time-domain measurements

Pump-probe delay scans are recorded with the Lund XUV-picosecond radiation source. As an example an exponentially decaying trace is shown in Fig. 1 for the $L^1\Pi$, $v = 0$ state of $^{12}\text{C}^{16}\text{O}$, where each data point represents 30 s of data collection, corresponding to averaging over 300 laser pulses.

The linewidth of the laser prevents from resolving any rotational structure and its center wavelength is set to cover the Q-branch in its entirety. The uncertainty of the data points, predominantly originating in Poissonian counting noise [6], is indicated with error bars in Fig. 1.

The data and their uncertainties are treated to derive decay transients in fitting procedures, where convolution of the instrument function is ac-

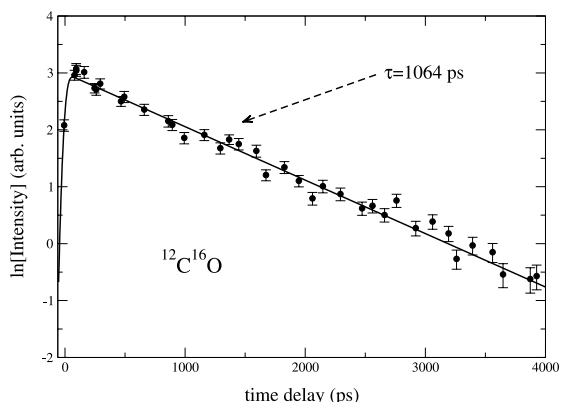


Fig. 1. Measurement of the pump-probe decay transient with the picosecond XUV-laser set at the unresolved Q-branch of the $L-X(0,0)$ band of $^{12}\text{C}^{16}\text{O}$.

Table 1
Lifetimes τ of the $L^1\Pi$ state (f-parity) of CO with estimated uncertainties

		τ (ps)	Unc.
$L^1\Pi, v = 0$	$^{12}\text{C}^{16}\text{O}$	1080 ^a	50
	$^{13}\text{C}^{16}\text{O}$	72 ^b	10
	$^{13}\text{C}^{18}\text{O}$	29 ^c	6
$L^1\Pi, v = 1$	$^{12}\text{C}^{16}\text{O}$	<70 ^d	

^a Value derived from time-domain measurement; frequency-domain data demonstrate the J -independence of the lifetime.

^b Derived from frequency-domain data; values pertain to $J = 1$ –9; τ independent of J in this range, consistent with time-domain data.

^c Derived from frequency-domain data; consistent with an upper limit of time-domain data.

^d Estimated from time-domain data.

counted for. The results for the data of Fig. 1 yield a lifetime of 1064 ps. Averaging over a number of data sets yields a value for the lifetime with an estimated error, which is listed in Table 1, where all results of the lifetime measurements are summarized.

In Fig. 2 a similar decay is shown for the $L^1\Pi, v = 0$ state of the $^{13}\text{C}^{16}\text{O}$ isotopomer. The decay in this case is much shorter (82 ps) and the instrument function in the fitting procedure affects the result. For the purpose of a proper fitting procedure the recording of data at negative delays is important. In the case of the $^{13}\text{C}^{18}\text{O}$ isotopomer the lifetime is even shorter to an extent, where no reliable value

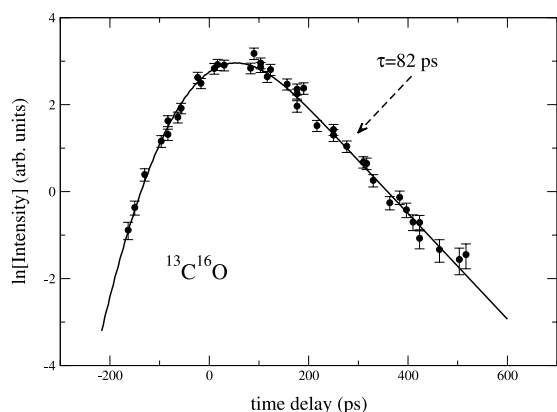


Fig. 2. Measurement of the pump–probe decay transient with the picosecond XUV-laser set at the unresolved Q-branch of the L – $X(0,0)$ band of $^{13}\text{C}^{16}\text{O}$.

for the lifetime can be given. Only an upper limit of 70 ps is derived from these measurements.

The signal for the $L^1\Pi, v = 1$ of $^{12}\text{C}^{16}\text{O}$ is found to be very weak and the registered spectrum shows a peak around $105410 \pm 8 \text{ cm}^{-1}$. This value agrees well with the value for the bandhead at 105405 cm^{-1} , as reported by Casey [21]; no structure is found at the value of 105440 cm^{-1} given for the bandhead in [22]. Again only an upper limit of 70 ps for the lifetime could be given in this case.

3.2. Frequency-domain measurements

High resolution XUV-excitation spectra are obtained with the narrow-band XUV-laser system in Amsterdam. Here are documented the results for the $4p\pi L^1\Pi, v = 0$ state of three different isotopomers. Some small signals are observed for the $4p\pi L^1\Pi, v = 1$ state, but these are too weak to perform spectroscopic assignments.

3.2.1. $^{12}\text{C}^{16}\text{O}$

Typical spectra for the L – $X(0,0)$ band of the main $^{12}\text{C}^{16}\text{O}$ isotopomer are displayed in Fig. 3. Previously, using the same setup, similar spectra were obtained under conditions aiming for the highest spectral resolution [11].

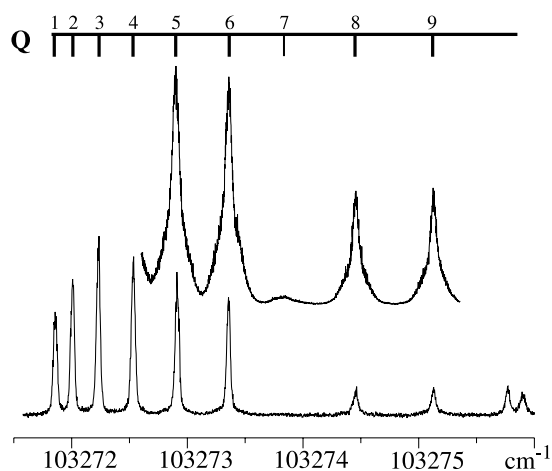


Fig. 3. Excitation spectra of the Q-branch of the L – $X(0,0)$ band in $^{12}\text{C}^{16}\text{O}$ via 1 XUV+1 UV photoionization with the narrow-band laser setup. The upper spectrum is recorded at higher density in the beam giving rise to pressure build-up in the detection chamber and a Doppler-broadened pedestal in the spectrum.

In the present measurements these conditions are relaxed; higher densities in the molecular beam are used and the nozzle–skimmer distance is decreased. As a consequence the lines broaden and the pressure build-up in the interaction chamber gives rise to a pedestal in the lineshape, as is clearly observable in the upper panel in Fig. 3 recorded at the highest pressure settings. But as a result the Q(7) line, which was absent in all previous studies [11,13], appears as a broad and shifted resonance indicative of the occurring perturbation. Moreover, at the highest densities somewhat higher rotational lines in the Q-branch can be recorded as well, allowing for a more detailed spectral analysis. In the lower panel of Fig. 3, the shape of the Q lines is Lorentzian with a corresponding width of 1100 MHz. Considering the known lifetime of these levels (150 MHz) the apparatus width is estimated at 950 MHz. Some attempts have been done to reduce this width by increasing the nozzle–skimmer distance and decreasing the backing pressure. These conditions yields to colder temperature in the beam and a limit of 700 MHz for the width of Q lines corresponding to 550 MHz for the apparatus width. Absolute frequencies, obtained from previously described calibration procedures [11] using saturated I₂-resonances and etalon markers are listed in Table 2, where also previous values are included. Frequency separations between adjacent Q-branch lines, which can be determined with higher precision are given in Table 3. For completeness high-resolution data on two R-branch lines are added in Table 2.

The data on the absolute transition frequencies and the more accurate relative frequencies for the Q-branch lines are included in a least-squares spectroscopic analysis. The ground state rotational levels are calculated from the most accurate rotational constants, for ¹²C¹⁶O reported by Varberg and Evenson [23].

The excited state rotational levels are represented, in a first analysis, by

$$E_{e,f}^L(J) = v_0 + B_{e,f}J(J+1) - D_{e,f}J^2(J+1)^2 \quad (1)$$

for both e and f-parity levels. In this procedure, that was already followed with a limited data set in [11], a perturbation results in the form of shifts in

Table 2

Transition frequencies of the Q-branch and R-branch lines in the L–X(0,0) band of ¹²C¹⁶O and deviations obtained in various a least-squares fit procedures

<i>J</i>	Frequency	Unc.	Δ _{unp}	Δ _s
1	103 271.8641	0.003	0.0031	0.0002
2	103 272.0134	0.003	0.0030	0.0001
3	103 272.2369	0.003	0.0025	–0.0005
4	103 272.5363	0.003	0.0033	0.0000
5	103 272.9097	0.003	0.0037	–0.0008
6	103 273.3620	0.003	0.0086	–0.0009
7	103 273.8293	0.005	–0.0456	0.0002
8	103 274.4611	0.004	–0.0093	–0.0001
9	103 275.1330	0.004	–0.0066	–0.0004
10	103 275.8799	0.005	–0.0025	0.0029
11	103 276.6938	0.005	–0.0047	0.0003
12	103 277.5828	0.005	–0.0045	–0.0001
13	103 278.5460	0.005	–0.0032	0.0009
14	103 279.5828	0.005	–0.0003	0.0029
15	103 280.6854	0.005	–0.0037	–0.0015
16	103 281.8616	0.005	–0.0050	–0.0043
17	103 283.27	0.100	0.084	–0.084
18	103 284.62	0.100	0.115	–0.112
19	103 286.03	0.100	0.135	0.130
20	103 287.50	0.100	0.146	0.136
22	103 290.66	0.100	0.181	0.160
<i>R</i> (<i>J</i>)	Unc.	Δ		
0	103 275.7524	0.0030	0.0015	
1	103 279.8336	0.0030	0.0001	

For the Q-branch, data for *J* > 17 are taken from [10], while the data for *J* ≤ 16 are averages from the present work and the results of [11]. Δ_{unp} are the deviations from a least-squares fit to an unperturbed Q-branch. Δ_s represent the deviations in a model where a single perturber state is included. For the R-branch, Δ represent the deviation from a least-squares analysis in which data of [10] are included. All values in cm^{–1}.

energy levels, calculated and listed in Tables 2 and 3 in the column displaying Δ_{unp}. Subsequently an analysis is performed with a perturber state represented by a similar formula for the rotational levels as Eq. (1) and put in a 2 × 2 interaction matrix:

$$M_f = \begin{pmatrix} E_f^L(J) & W_{\text{int}} \\ W_{\text{int}} & E_{\text{pert}}(J) \end{pmatrix} \quad (2)$$

with a *J*-independent interaction term *W*_{int} representing a homogeneous perturbation with some unknown state. The local perturbation is only invoked for the f-parity components and it is verified that a heterogeneous perturbation do not give any

Table 3

Differences between frequencies of the Q-branch lines in the L–X(0,0) band of $^{12}\text{C}^{16}\text{O}$, measured in relative terms with respect to etalon traces and deviations obtained in the least-squares fit procedures

Lines	Diff.	Unc.	Δ_{unp}	Δ_s
Q(1)–Q(2)	4474	8.	–5.	–5.
Q(2)–Q(3)	6709	8.	–7.	–10.
Q(3)–Q(4)	8960	10.	8.	–1.
Q(4)–Q(5)	11 214	10.	31.	–4.
Q(5)–Q(6)	13 566	10.	155.	4.
Q(6)–Q(7)	14 010	50.	–1624.	31.
Q(7)–Q(8)	18 966	40.	1115.	20.
Q(8)–Q(9)	20 162	15.	98.	10.
Q(9)–Q(10)	22 313	15.	45.	18.
Q(10)–Q(11)	24 439	25.	–25.	–39.
Q(11)–Q(12)	26 657	40.	5.	–7.
Q(12)–Q(13)	28 868	40.	38.	22.
Q(13)–Q(14)	31 082	45.	83.	60.
Q(14)–Q(15)	33 060	70.	–95.	–127.
Q(15)–Q(16)	35 261	70.	–40.	–84.

Δ_{unp} are the deviations from an unperturbed Q-branch. Δ_s represent the deviations in a model where a single perturber state is included. All values in MHz.

improvement. The high resolution data, allowing observation of shifts on $J = 7$, but also on neighboring J -values, give good confidence in the effective band origin and rotational B constant for the perturber state. This analysis results in a set of molecular constants, which are listed in Table 6, and a new set of deviations from the fit, which are again included in Tables 2 and 3 in the column displaying Δ_s . Improved constants for the e-parity states are also included in Table 6. For the f-parity components some discrepancies seem to remain at $J = 10$ and $J = 15$. This suggests an analysis with perturbation with the three components of a triplet ($^3\Pi$ or $^3\Delta$). An unsuccessful attempt was made to model such a perturbation, assuming homogeneous or heterogeneous coupling.

3.2.2. $^{13}\text{C}^{16}\text{O}$

A typical spectrum of the Q-branch in the L–X(0,0) band of $^{13}\text{C}^{16}\text{O}$ is shown in Fig. 4; it is the first time that this Q-branch is resolved. Clearly visible is the much larger linewidth in $^{13}\text{C}^{16}\text{O}$ compared to the main $^{12}\text{C}^{16}\text{O}$ isotopomer. Transition frequencies of the individual, slightly overlapping, resonances are determined by comparison with etalon markers and the I_2 -saturated spectrum

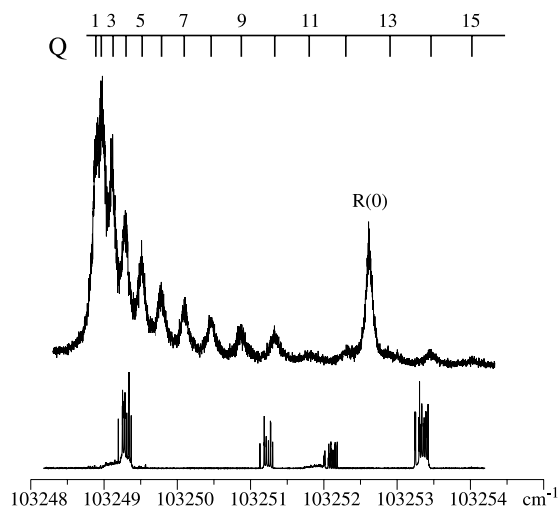


Fig. 4. Excitation spectra of the Q-branch of the L–X(0,0) band in $^{13}\text{C}^{16}\text{O}$. In the lower panel the simultaneously recorded saturated I_2 -spectrum is displayed, which was used for absolute frequency calibration.

[20], but in view of the linewidth the accuracy is somewhat reduced. Results for Q-branch and R-branch lines are listed in Table 4.

As a result of the larger linewidth in $^{13}\text{C}^{16}\text{O}$ the individual lines in the Q-branch are not entirely resolved at the bandhead, hence simple counting of lines as in $^{12}\text{C}^{16}\text{O}$ is not feasible. Because of the perturbation in the Q-branch various fitting procedures do not give an unambiguous identification either. To produce further evidence a spectrum was recorded at lower temperature in the molecular beam. From Fig. 5 we conclude with good confidence that our numbering is correct.

A spectroscopic analysis of the transition frequencies is performed, using ground state constants of Guelachvili et al. [24], and representing the excited state with Eq. (1). Resulting deviations are given in Table 4 in the column Δ_{unp} . The corresponding molecular constants are given in Table 6. Again, similarly as for $^{12}\text{C}^{16}\text{O}$ small deviations remain, indicative of weak perturbation effects.

In addition, an accidental perturbation is clearly visible for Q(11) with a sudden drop of the intensity of the line. Q(12) and Q(13) are partially blended by the R(0) component, but Q(14) appears with a regular intensity, assuming a Boltzmann distribution in the molecular beam. Hence both

Table 4
Transition frequencies of the Q-branch and R-branch lines in the L–X(0,0) band of $^{13}\text{C}^{16}\text{O}$ (values in cm^{-1})

J	$Q(J)$	Unc.	Δ_{unp}
1	103 248.8828	0.009	0.006
2	103 248.9727	0.005	0.005
3	103 249.1129	0.005	0.009
4	103 249.2884	0.005	0.002
5	103 249.5114	0.005	–0.002
6	103 249.7804	0.005	–0.005
7	103 250.0972	0.005	–0.003
8	103 250.4630	0.009	0.004
9	103 250.8684	0.009	0.008
10	103 251.3327 ^a	0.009	0.029
11	103 251.8019	0.015	0.014
12	103 252.3168	0.010	0.004
14	103 253.4509	0.010	–0.025
15	103 254.0222 ^a	0.015	–0.092

$R(J)$	Δ	Γ (GHz)		
0	103 252.6208	0.006	0.012	2.31
1	103 256.4884	0.006	–0.002	2.58
2	103 260.4584	0.006	–0.008	2.78
3	103 264.64			3.95

Δ represents the deviation from a least-squares analysis of the data and Γ the natural linewidths for the R-branch. $\Gamma = 2.2$ GHz is measured independent of J for the Q-branch from 1 to 9.

^a Left out of the least-squares fit.

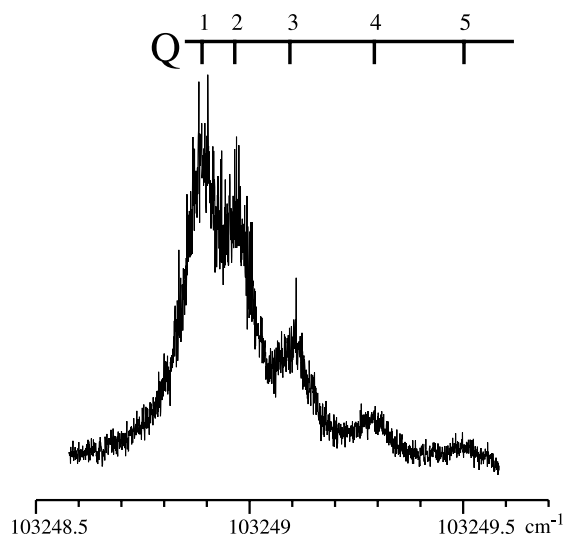


Fig. 5. Detail of the Q-branch bandhead for $^{13}\text{C}^{16}\text{O}$, recorded at lower temperatures in the molecular beam, and giving evidence for the rotational assignment of low J -states.

the spectral and the intensity analysis are consistent in indicating a perturbation at around $J = 10$ – 11 ; we note here that an intensity decrease in 1 XUV + 1 UV photoionization is associated with the phenomenon of predissociation [10].

For the e-parity component of $^{13}\text{C}^{16}\text{O } 4p\pi L^1\Pi$, $v = 0$ the transition frequencies and linewidths of R(0)–R(3) lines have been determined by the same procedures. The transition frequencies are included in the least-squares fit, with inclusion of the data of [10], and using only one value for ν_0 for both parity components. The resulting rotational constants are listed in Table 6.

The linewidths of the Q-branch lines of $^{13}\text{C}^{16}\text{O}$ are analyzed as well. By fitting to a Lorentzian line profile and deconvoluting for the instrumental linewidth, a value for the natural width Γ associated with the lifetime of the upper state, is found for the different J values. No rotational dependence is found. From the spectrum of Fig. 5 a value of 2800 MHz for the measured linewidth of Q(1)–Q(4) lines give natural linewidth of 2250 MHz considering the instrumental linewidth of 550 MHz for the cold molecular beam conditions. From the spectrum of Fig. 4, a larger value of 3150 MHz is found for the measured width for Q(1)–Q(9), but the deconvolution width of 950 MHz which has to be applied for the warmer molecular beam conditions keeps the coherent value of 2200 MHz for the natural linewidth. Assuming an uncertainty of 300 MHz, the corresponding lifetime is 72 ± 10 ps. This value is consistent with $\tau = 82 \pm 15$ ps found in time-domain measurements for the Q-branch, in view of the fact that the latter measurements are performed at the end of the dynamic range of the instrument. Hence we adopt a value of 72 ± 10 ps for the f-components of $^{13}\text{C}^{16}\text{O } 4p\pi L^1\Pi$, $v = 0$ in Table 1.

Deconvoluted linewidths for some low- J R-branch lines are included in Table 4. The gradual decrease of lifetime with increasing J , which was not observed previously [10], follows the trend as in $^{12}\text{C}^{16}\text{O}$, but the effect is smaller. Analysis of the predissociation rate k ($k = 2\pi\Gamma$) with

$$k_p(J) = k_0 + k_p J(J + 1) \quad (3)$$

yields values of $k_0 = 1.4 \times 10^{10} \text{ s}^{-1}$ and $k_p = 3 \times 10^8 \text{ s}^{-1}$ for the e-components of $^{13}\text{C}^{16}\text{O}$

$4p\pi L^1\Pi$, $v = 0$. This is a much slower increase, compared to $^{12}\text{C}^{16}\text{O}$, and at $J = 14$ this would yield a width of only 12 GHz, explaining why it was not observed in the lower resolution study of [10].

3.2.3. $^{13}\text{C}^{18}\text{O}$

A spectrum for the Q-branch of the L–X(0,0) band of the $^{13}\text{C}^{18}\text{O}$ isotopomer is shown in Fig. 6. In the spectrum two bandheads appear; the low- J bandhead is red-degraded in contrast to the case of $^{12}\text{C}^{16}\text{O}$ and $^{13}\text{C}^{16}\text{O}$. The pile-up of high- J lines is increased in the spectrum recorded at a somewhat higher rotational temperature in the molecular beam.

Some newly observed and calibrated R lines are given in Table 5.

The analysis of the data on the line positions is made as follows: the molecular constants listed in Table 6 are obtained including only the low J values ($J < 9$) for both parities and keeping constant the D values at 1×10^{-5} . As the lowest J values of the Q-branch are again not resolved, the line broadening being even stronger than in $^{13}\text{C}^{16}\text{O}$, we have attempted fits with different

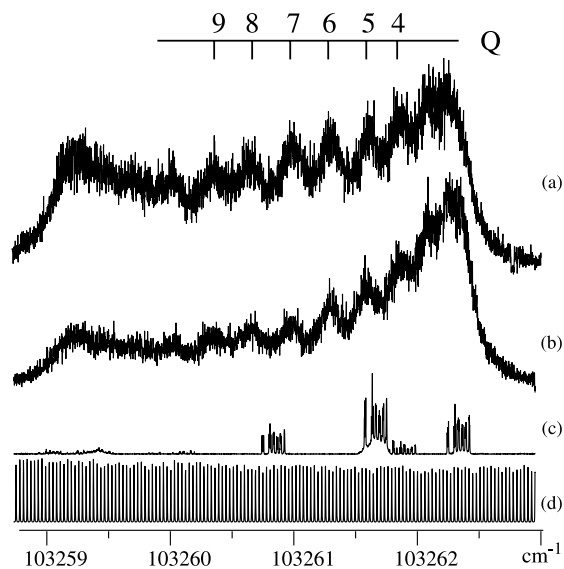


Fig. 6. (a) Excitation spectra of the Q-branch of the L–X(0,0) band in $^{13}\text{C}^{18}\text{O}$; (b) same spectrum recorded at lower temperature in the molecular beam; (c) saturated I_2 -spectrum; (d) etalon markers.

Table 5

Transition frequencies of the Q-branch and R-branch lines in the L–X(0,0) band of $^{13}\text{C}^{18}\text{O}$ (values in cm^{-1})

J	$Q(J)$	Unc.	Δ_{unp}
1	103 262.311	0.100	0.022
2	103 262.292	0.100	0.117
3	103 262.082	0.100	0.061
4	103 261.850	0.010	0.022
5	103 261.600	0.010	0.007
6	103 261.295	0.010	–0.020
7	103 260.982	0.010	–0.012
8	103 260.636	0.010	0.010
9	103 260.341	0.100	0.130

$R(J)$	Unc.	Δ	Γ (GHz)	
0	103 265.929	0.010	0.015	5.0
1	103 269.438	0.010	–0.004	5.1
2	103 272.967	0.010	–0.020	5.1

Γ is the natural linewidth for the R-branch lines. A J -independent value of $\Gamma = 5.4$ GHz is derived for the overlapping Q-branch components.

numbering of the six resolved Q components. The final assignment of these Q-branch lines, as given in Table 5 is only tentative; the lines may well be shifted by a quantum of rotation.

Table 6

Molecular constants for e and f-components of the $L^1\Pi$, $v = 0$ state as obtained from least-squares fits to the data and derived (1σ) uncertainties

		Value (cm^{-1})
$^{12}\text{C}^{16}\text{O}$	ν_0	103 271.7866(10)
	B_f	1.959841(10)
	D_f	$0.706(5) \times 10^{-5}$
	W_{int}	0.219 (3)
	ν_{pert}	103 267.602(10)
	B_{pert}	2.0561(2)
$^{13}\text{C}^{16}\text{O}$	B_e	1.98196(40)
	D_e	$1.5(4) \times 10^{-5}$
	ν_0	103 248.8295(3)
	B_f	1.86086(10)
$^{13}\text{C}^{18}\text{O}$	B_e	1.88948(50)
	D_f	$0.92(5) \times 10^{-5}$
	D_e	$6.7(3) \times 10^{-5}$
	ν_0	103 262.383(10)
	B_f	1.722(1)
	B_e	1.757(1)
	$D_{e,f}$	1.0×10^{-5a}

^a Value kept fixed in the fit.

Values for natural linewidths of some e-parity components of $^{13}\text{C}^{18}\text{O } 4p\pi\text{L}^1\Pi, v = 0$ are determined from an analysis of linewidths of R-branch lines. Values for $J = 1\text{--}3$ are included in Table 5. The overlapping structures of the Q-branches are analyzed also to derive linewidths of 5.4 GHz after deconvolution of the instrument width. This allows for a reasonable accurate estimation of the upper state lifetime of the f-parity components of the $4p\pi\text{L}^1\Pi, v = 0$ in $^{13}\text{C}^{18}\text{O}$, which is included in Table 1.

4. Discussion and conclusion

In the present study highly accurate data have been obtained for lifetimes, in some cases rotational-state dependent, and on transition frequencies pertaining to the $4p\pi\text{L}^1\Pi, v = 0$ state of $^{12}\text{C}^{16}\text{O}$, $^{13}\text{C}^{16}\text{O}$ and $^{13}\text{C}^{18}\text{O}$. Various phenomena of perturbations in the excited state are found, that are all connected to predissociation. For $^{12}\text{C}^{16}\text{O}$ and $^{13}\text{C}^{16}\text{O}$ the mechanisms are similar in a qualitative sense. The e-parity components undergo coupling with the $\text{D}^1\Sigma^+$ repulsive state, giving rise to a J -dependent interaction and a J -dependent predissociation rate, represented by k_J in Eq. (3). Here this phenomenon is found for $^{13}\text{C}^{16}\text{O}$ as well and a value for k_J is determined for the first time. The fact that it is much smaller than in $^{12}\text{C}^{16}\text{O}$ [10], indicates that coupling with $\text{D}^1\Sigma^+$ is weaker.

The discrepancy in the values for the lifetimes of the f-parity components in $^{12}\text{C}^{16}\text{O}$, 1.0 ± 0.3 ns in [11] and 0.55 ± 0.04 in [12], both obtained through line broadening measurements, seems to be resolved now, by independent time-domain measurements, in favor of the largest value with 1.08 ± 0.05 ns. Previously it has been hypothesized that the f-parity components in $^{12}\text{C}^{16}\text{O}$ might dominantly decay via radiation [11], but the work of Okazaki et al. [15,16], using detection of atomic fragments, shows that the f-components undergo strong predissociation, although at a rate less than the e-components.

Additionally a J -independent predissociation is found, represented by k_0 in Eq. (3), which should hold equally for e and f states, as discussed by

Okazaki et al. [16]. This effect is much stronger in $^{13}\text{C}^{16}\text{O}$ ($k_0 = 1.4 \times 10^{10} \text{ s}^{-1}$) than in $^{12}\text{C}^{16}\text{O}$ ($k_0 = 1.9 \times 10^9 \text{ s}^{-1}$), almost by an order of magnitude. It is not evident what the underlying mechanism is for this predissociation channel. Rostas et al. [25] have pointed at the strong interaction between $\text{L}^1\Pi, v = 0$ with other $^1\Pi$ states, most notably $\text{L}^1\Pi$ at 103211.8 cm^{-1} in $^{12}\text{C}^{16}\text{O}$. In $^{13}\text{C}^{16}\text{O}$ the band origin of the $\text{L}^1\Pi$ state is identified at 103161 cm^{-1} [10]. Following the analysis of [25] the $\text{L}^1\Pi, v = 0$ state in $^{12}\text{C}^{16}\text{O}$ is blue-shifted by the interaction with $\text{L}^1\Pi$; in $^{13}\text{C}^{16}\text{O}$ the band origin of the $\text{L}^1\Pi$ perturber is further to the red, indicating a weaker interaction. If the $\text{L}^1\Pi$ state would also be the origin of the perturbation of the f-component in $\text{L}^1\Pi, v = 0$, the effect would hence be expected to be weaker in $^{13}\text{C}^{16}\text{O}$, which is not the case.

As follows from the investigations by Okazaki et al., in addition to the usual dissociative singlet channel $\text{C}^3\text{P} + \text{O}^3\text{P}$, the triplet channel $\text{C}^1\text{D} + \text{O}^3\text{P}$ is effective for dissociation of $\text{L}^1\Pi, v = 0$ and $\text{L}^1\Pi, v = 1$ states in $^{12}\text{C}^{16}\text{O}$. The parameter k_0 is then distributed in singlet and triplet contributions [16]. Okazaki et al. have modeled empirically the competition between decay in singlet and triplet channels. In particular the f-parity components are coupled to the triplet channel. This is deduced from the fact that excitation of the Q-branch gives a strong signal in C^1D products. From an ab initio point of view this mechanism may be caused by repulsive valence states of triplet character. Such potentials have been calculated by O'Neil and Schaefer [18] and their $3^3\Pi$ and $2^3\Sigma^-$ are found to cross the potential of Rydberg states near their bottom. In contrast the e-parity component mainly results in C^3P products, so decay proceeds through the singlet channel. Apart from the coupling with the $\text{D}^1\Sigma^+$ state, yielding a J -dependent effect there is also a J -independent predissociation channel of singlet character. This may attributed to the repulsive $^1\Pi$ state, which was calculated in detail by Hiyama and Nakamura [17]. Hence four different predissociation mechanisms are required to account for the decay of the $\text{L}^1\Pi, v = 0$ state in $^{12}\text{C}^{16}\text{O}$: repulsive states of $^1\Pi$ and $^3\Pi$ character, the $\text{D}^1\Sigma^+$ state, and a bound state causing the accidental predissociation. This

makes the $L^1\Pi$, $v = 0$ state a benchmark system for studies in predissociation.

In addition, Okazaki et al. [16] mention that no $C(^1D)$ fragment was detected for higher Rydberg states, indicating the unique situation of L and L' versus the spin forbidden dissociative channel. Photofragment detection experiment for other isotopomers would certainly help solving the issue of the predissociation mechanisms.

In both $^{12}C^{16}O$ and $^{13}C^{16}O$ isotopomers additional local perturbations occur, which are associated with accidental predissociation. The $J = 7(f)$ level in $^{12}C^{16}O$ is a marked example studied before [11,13], but now the broadened line has been observed directly for the first time. Further local effects seem to occur at $J = 10$ and 15 for both $^{12}C^{16}O$ and $^{13}C^{16}O$, although the line shifts are too small for an unambiguous analysis. The nature of the perturber state for these accidental perturbations has yet to be identified.

The situation in $^{13}C^{18}O$ seems to be different. A J -dependent lifetime for e-parity components is not observed, but that may be attributed to the fact that the J -independent channel (k_0) is rather large. As was discussed in [25] another state of $^1\Pi$ symmetry, also observed by Eikema et al. [26], is located in the energy region of the $4p\pi$ – $4p\sigma$ complex. The $^1\Pi$ state, identified at $103\,203.07\text{ cm}^{-1}$, is presumed to interact with the $L^1\Pi$, $v = 0$ state in $^{13}C^{18}O$. In the study of [10] the lines of the extra $^1\Pi$ state are found to be rather narrow, so this feature may well be the cause of an overall shift of $L^1\Pi$, $v = 0$, but it is for this reason not likely to be the origin of the J -independent predissociation. This shift is clearly not in the way of explaining the red-degraded Q-branch and an explanation for this feature need to treat at least for the f parity the three $^1\Pi$ states known in the energy range.

The right answer to explain all these features observed in the energy region of the $4p\pi$ – $4p\sigma$ complex will be to treat in a comprehensive deperturbation analysis all interacting states, accounting for shifts and predissociations. Such an analysis, which is outside the scope of the present experimental study, is currently being performed [27].

We note that the local rotational analyses performed here should be considered preliminary.

The representation of the accidental predissociation near $J = 7$ for f-components in $^{12}C^{16}O$ gives satisfactory agreement on the perturbed line positions. However, the resulting B -constant for the unknown perturber state is unphysical, indicating that this phenomenon is more complex. The same holds for the rotational analyses and even the identification of Q-branch lines in $^{13}C^{16}O$ and $^{13}C^{18}O$. By no means a regular fit can be produced when all data are included. For a limited set of rotational lines a converging fit can be produced. But still shifting the rotational identification by one quantum gives reasonable agreement. Also here only a comprehensive treatment, including perturbations by a number of perturbing states in the $4p$ region can produce a proper picture. Then the additional line positions at high J -values may be of help, since that is where the perturbations are strongest. It should be understood that the numbering of quantum states in the Q-branches of the heavier isotopomers cannot be accomplished by trying to further resolve the spectra; the limit of the natural lifetime is reached. However, a possibility could be to perform a high-resolution double-resonance experiment, in which certain rotational quantum states are prepared and the number of lines reduced. Selection rules then would allow for an unambiguous identification.

Acknowledgements

P.C. and W.U. wish to thank the Lund Laser Centre for their hospitality. The work in Lund was supported by the European Community - Access to Research Infrastructures action of the Improving Human Potential Programme, Contract No. HPRI-CT-1999-00041. P.C. and A.J. wish to thank the Laser Centre Vrije Universiteit for their hospitality. The work in Amsterdam was supported by the European Community - Access to Research Infrastructures action of the Improving Human Potential Programme, Contract No. HPRI-CT-1999-00064. The authors wish to thank K.P. Huber (NRC Ottawa) for advice and for critically reading the manuscript. Financial support from the Netherlands Foundation for Research of Matter (FOM) is gratefully acknowledged.

References

- [1] K.P. Huber, *Philos. Trans. R. Soc. London A* 355 (1997) 1527.
- [2] C. Letzelter, M. Eidelsberg, F. Rostas, J. Breton, B. Thieblemont, *Chem. Phys.* 114 (1987) 273.
- [3] Y.P. Viala, C. Letzelter, M. Eidelsberg, F. Rostas, *Astron. Astrophys.* 193 (1988) 265.
- [4] G.L. Wolk, J.W. Rich, *J. Chem. Phys.* 79 (1983) 12.
- [5] E.F. van Dishoeck, J.H. Black, *Astrophys. J.* 334 (1988) 771.
- [6] P. Cacciani, W. Ubachs, P.C. Hinnen, C. Lyngå, A. L’Huillier, C.-G. Wahlström, *Astrophys. J.* 499 (1998) L223.
- [7] W. Ubachs, I. Velchev, P. Cacciani, *J. Chem. Phys.* 113 (2000) 547.
- [8] P. Cacciani, F. Brandi, I. Velchev, C. Lyngå, C.-G. Wahlström, W. Ubachs, *Eur. J. Phys. D* 15 (2001) 47.
- [9] P.F. Levelt, W. Ubachs, W. Hogervorst, *J. Chem. Phys.* 97 (1992) 7160.
- [10] K.S.E. Eikema, W. Hogervorst, W. Ubachs, *Chem. Phys.* 181 (1994) 217.
- [11] W. Ubachs, K.S.E. Eikema, W. Hogervorst, P.C. Cacciani, *J. Opt. Soc. Am. B* 14 (1997) 2469.
- [12] M. Drabbels, W.L. Meerts, J.J. ter Meulen, *J. Chem. Phys.* 99 (1993) 2352.
- [13] S. Sekine, T. Masaki, Y. Adachi, C. Hirose, *J. Chem. Phys.* 89 (1988) 3951.
- [14] M. Komatsu, T. Ebata, T. Maeyama, N. Mikami, *J. Chem. Phys.* 103 (1995) 2420.
- [15] A. Okazaki, T. Ebata, T. Sutani, N. Mikami, *J. Chem. Phys.* 108 (1998) 1765.
- [16] A. Okazaki, T. Ebata, N. Mikami, *J. Chem. Phys.* 114 (2001) 7886.
- [17] M. Hiyama, H. Nakamura, *Chem. Phys. Lett.* 248 (1996) 316.
- [18] S.V. O’Neil, H.F. Schaefer III, *J. Chem. Phys.* 53 (1970) 3994.
- [19] W. Ubachs, K.S.E. Eikema, P.F. Levelt, W. Hogervorst, M. Drabbels, W.L. Meerts, J.J. ter Meulen, *Astrophys. J.* 427 (1994) L55.
- [20] I. Velchev, R. van Dierendonck, W. Hogervorst, W. Ubachs, *J. Mol. Spectrosc.* 187 (1998) 21.
- [21] M. Casey, Ph.D. Thesis, University College Dublin, Ireland, 1978.
- [22] M. Eidelsberg, F. Rostas, *Astron. Astrophys.* 235 (1990) 472.
- [23] T.D. Varberg, K.M. Evenson, *Astrophys. J.* 385 (1992) 763.
- [24] G. Guelachvili, D. de Villeneuve, R. Farrenq, W. Urban, J. Vergès, *J. Mol. Spectrosc.* 98 (1983) 64.
- [25] F. Rostas, F. Launay, M. Eidelsberg, M. Benharrous, C. Blaess, K.P. Huber, *Can. J. Phys.* 72 (1994) 913.
- [26] K.S.E. Eikema, W. Hogervorst, W. Ubachs, *J. Mol. Spectrosc.* 163 (1994) 19.
- [27] K.P. Huber, private communication.